Published by JScE as Proceedings of 4th International Conference on Role of Energy on Sustainable Social Development (RESSD-2025), 29-30 May, 2025, Kathmandu, Nepal

POWER SHARING CONTROL STRATEGY IN AC MICROGRID SYSTEM CONSISTING OF RENEWABLE ENERGY SOURCES

Abinash Kshatri[1]*, Sandeep Dhami[1], Amrit Bhatta[1]

[1] Department of Electrical Engineering, IOE-Pashchimanchal Campus,Tribhuvan University

Abstract

Addressing the need for reliable off-grid electricity in regions like Nepal, this paper investigates a power sharing control strategy for an islanded AC microgrid comprising a 60 kW micro-hydropower (MHP) unit and a 33.4 kW solar photovoltaic (PV) system. The proposed strategy employs a swing equation-based droop controller for the PV inverter to emulate synchronous generator inertia and facilitate dynamic power sharing with the MHP, which is managed by conventional governor and excitation controls. System performance was evaluated using MATLAB/Simulink under significant load variations, including a 20 kW active power step load and 5 kVAR reactive power step. The results demonstrate the system's ability to maintain the frequency deviation within ±1% of 50 Hz and the voltage deviation within 4.9%, ensuring robust stability and effective load allocation. This research contributes to a validated control approach and detailed performance analysis for a batteryless MHP-PV hybrid configuration, offering practical insights for deploying sustainable and stable decentralized energy systems in remote geographical locations.

Keywords: Swing equation-based droop control, Hybrid AC microgrid, Power sharing control, Energy synchronization.

1. Introduction

The global movement towards more environmentally friendly energy sources has increased interest in renewable power sources for electricity generation (Ayres and Zamora, 2024). Due to their off-grid or distant locations, microgrids are now part of the grid infrastructure, enabling local distribution and grid resilience (Abu-Sharkh et al., 2006). With countries like Nepal, which have abundant hydroelectric resources and high solar irradiance, adopting increasing levels of microgrid deployment to support energy access, development, and sustainability, these microgrids integrate various renewable energy sources to effectively meet local energy demands (Bhattarai et al., 2024). However, the full exploitation of renewable energy sources in microgrids is based on robust power sharing control schemes to ensure reliable grid stability, efficient resource utilization, and seamless integration of distributed generation assets (Badal et al., 2019). Legacy centralized power systems struggle to handle the variability and intermittency of renewables , thus requiring new control methods tailored for the microgrid environment to offer dynamic coordination of sources, grid synchronization, and load prioritization with minimal energy losses and ecological impact (Badal et al., 2019).

The concurrent interconnectedness of various renewable sources in microgrids requires stringent synchronization processes in terms of grid connection to provide optimal performance, especially in island-mode operations where local power creation is essential (Yan et al., 2019, Fachini et al., 2024). The innate fluctuation in renewable sources combined with variable energy demands increases the challenges in distributing power, consequently demanding the use of adaptive controllers with the ability to respond to changing situations and load profile changes. Effective power distribution to loads with an emphasis on maintaining priority demand maximization and minimizing losses is paramount to providing continuity in the supply of electricity. The complexity associated with multi-source microgrid systems consisting of distributed generations, energy storage (Amrollahi and Bathaee, 2017, Saranya et al., 2015, Alramlawi et al., 2018), as well as load response, presents serious challenges in the development of efficient control techniques. The centralization and

*Corresponding author: Abinash Kshatri
Department of Electrical Engineering, Pashchimanchal Campus, TU
Email: abinashkshatri123@gmail.com
https://doi.org/10.3126/jsce.v12i2.91426

deterministic nature of traditional grid operations are not in a position to handle such complexities; therefore, there is an urgent need to develop intelligent techniques to control distributed energy sources, maintain voltage and frequency stability, and provide reliable performance in different operating modes (Anderson and Fouad, 2008).

The effective integration of renewable energy sources into microgrids is heavily based on robust control strategies for power sharing and stability (Badal et al., 2019). Droop control is a well-established technique for managing power distribution among parallel photovoltaic (PV) inverters (Baral and Pun, 2022) .Furthermore, enhancing grid stability through virtual inertia provision from PV systems has become a significant research focus, particularly for low-inertia grids (Khazali et al., 2022). The application of advanced inertia-emulating controls in hybrid systems, such as those that combine photovoltaic power with micro-hydropower (MHP), has also been explored (Neupane and Gurung, 2022). However, a specific investigation into the dynamic performance of swing equation-based droop control for a hybrid MHP (60 kW) & PV (33.4 kW) islanded AC microgrid without battery storage, emphasizing the coordinated control required for stable operation and equitable power sharing between the synchronous MHP and the inertia-emulating PV inverter under significant load transients (20 kW active, 5 kVAR reactive steps) to meet stringent voltage ($\leq$ 4.9% *deviation*) and frequency ($\leq$ 1% *deviation*) targets, particularly in the context of remote Nepalese communities, offers a distinct contribution. This paper addresses this by:

1. Developing a detailed model of the MHP-PV hybrid system where the PV inverter utilizes swing equation-based droop control to provide virtual inertia and dynamically share load with the MHP unit.
2. Validating through comprehensive MATLAB/Simulink simulations the system's capability to maintain the defined stability criteria and achieve effective power sharing under dynamic load conditions.
3. Providing a practical case study with specific control parameters (virtual inertia J = 0.1028 pu, active power droop m = 0.0001) for this MHP-PV configuration, offering a reference for similar off-grid renewable energy projects .

2. Ease of Use Control Strategy Theories

This section outlines the control strategies employed for the 60 kW micro-hydropower (MHP) unit Usman and Abdulkadir, 2015 Acakpovi et al., 2014 and the 33.4 kW solar photovoltaic (PV) system within the standalone AC microgrid.

2.1. Theory Related to Micro Hydropower

2.1.1 Governor System (Turbine Control)

The governor system controls the mechanical power input to the MHP turbine by adjusting the water flow against frequency fluctuations. In an analysis based on PID, it stabilizes rotor speed (1500rpm) and provides a quick response to load variations. This controller plays a critical role in ensuring frequency stability (Acakpovi et al., 2014, Anderson and Fouad, 2008) and avoiding mechanical stress on the turbine during transient operation. Mathematically,PID-Based Governor,

$$\Delta P_m = K_p \Delta f + K_i \int \Delta f dt + K_d \frac{d\Delta f}{dt} \quad (1)$$

where, $\Delta f = f_{\text{ref}} - f_{\text{actual}}$(frequency deviation)

2.1.2 Excitation System of Synchronous Generator

The excitation system regulates the terminal voltage of the MHP's synchronous generator by regulating the rotor field current. It uses a PID controller to detect the actual terminal voltage and compare it with the reference value ($V_{ref.} = 400V$) and minimize error. The system ensures the stability of the voltage output under fluctuation of the load (Anderson and Fouad, 2008, Gieras, 2016, Ayasun et al., 2014) and synchronizes with the grid. Its reliability is critical to preventing voltage collapse and providing a stable power supply in isolated microgrids. Mathematically, PID controller

$$G_{\text{PID}}(s) = K_p + \frac{K_i}{s} + K_d s \quad (2)$$

where,$K_p = 33.46,\ K_i = 7978.96,\ K_d = -0.00998$

2.2. Solar PV System

2.2.1 Maximum Power Point Tracking (MPPT)

To maximize the energy extraction from the photovoltaic array under fluctuating environmental conditions, a Perturb and Observe (P&O) Maximum Power Point Tracking (MPPT) algorithm is implemented (Chauhan et al., 2022). This algorithm, detailed in Figure 1, adaptively adjusts the operating voltage of the photovoltaic array to track the Maximum Power Point (MPP). The PV voltage, operating at$V_{pv(MPP)}$, is then increased by a DC-DC boost converter to achieve the required DC link voltage ($V_{DC-link}$) for effective power delivery to the inverter. The boost converter, a critical switched-mode power electronic device whose

operation is detailed in (Erickson and Maksimovic, 2007), is controlled via its duty cycle. Mathematically,
Boost Converter duty cycle,

$$D = 1 - \frac{V_{PV}}{V_{DC-link}} \tag{3}$$

which is dictated by the MPPT output. This integrated approach significantly enhances overall system efficiency compared to non-MPPT systems (Chauhan et al., 2022). The power extracted by the MPPT is calculated as PV Power Calculation,

$$P_{PV} = V_{PV} \, . \, I_{PV} \tag{4}$$

where, $V_{PV(mpp)} = 29.3V \, (MPP \, voltage), V_{DC-link} = 400V$

2.2.2 PV Inverter (VSI) Control Strategy

The control architecture for the PV system's Voltage Source Inverter (VSI), detailed in Figure 2, is designed for stable grid integration, dynamic power sharing, and contribution to grid stability through virtual inertia. The control system operates in the synchronous d-q reference frame, synchronized with the Point of Common Coupling (PCC) voltage.

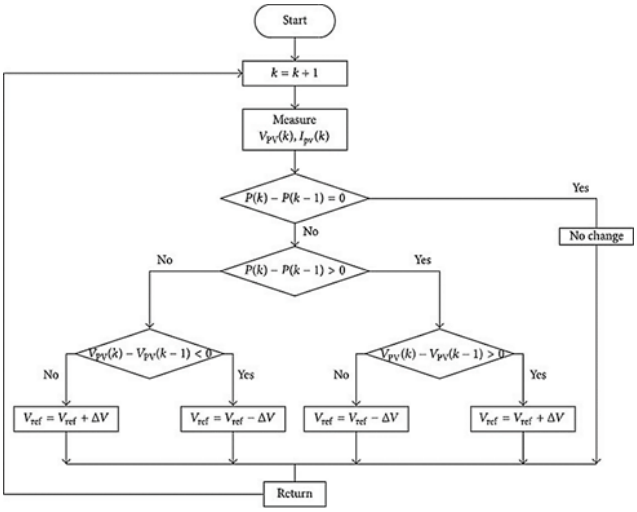

Figure 1. Flowchart of P & O algorithm

i. Grid Synchronization and Measurement
The VSI control system first determines the status of the grid through measurements at the PCC. A Phase-Locked Loop (PLL) processes the measured three-phase PCC voltage ($V_{\text{PCC(abc)}}$) to precisely estimate the instantaneous phase angle of the grid voltage (θ_{grid}) and the measured grid angular frequency ($\omega_{\text{grid(meas)}}$).The signal $\omega_{\text{grid(meas)}}$ is fundamental for frequency-dependent control actions Ali et al., 2018.Both ($V_{\text{PCC(abc)}}$) and the measured VSI output current ($I_{\text{VSI(abc)}}$ are transformed into the d-q frame using θ_{grid} via Park Transforms, yielding $V_{d(grid)}, V_{q(grid)}, I_{d(meas)},$ and $I_{q(meas)}$ (Martínez-Velasco, 2010, Anderson and Fouad, 2008, Martínez-Velasco, 2010, Anderson and Fouad, 2008).

ii. Realization of Droop Control
a.Active Power Control (Swing Equation & P-f Droop):
The realization of frequency droop with virtual inertia support occurs in this block in Figure 2. It directly addresses the frequency dynamics of the grid.The measured angular frequency of the grid ($\omega_{\text{grid(meas)}}$), obtained from the PLL, serves as the primary input. The frequency deviation from the nominal value ($\omega_{\text{grid(nominal)}}$) is calculated as:

$$\Delta\omega = \omega_{grid(meas)} - \omega_{nominal} \tag{5}$$

This deviation ($\Delta\omega$) drives the dynamics of the virtual synchronous generator swing equation, implemented as the swing equation,

$$J\frac{\mathrm{d}(\Delta\omega)}{\mathrm{d}t} = P_{\text{m(virtual)}} - P_{\text{e(PVmeas)}} - D\Delta\omega \tag{6}$$

$P_{\text{e(PVmeas)}}$ is the measured active power output of the VSI. The virtual mechanical power input term, $P_{\text{m(virtual)}}$, incorporates the P-f droop characteristic and the available power from the MPPT (P_{mppt}) . Modified Droop Law,

$$P_{\text{m(virtual)}} = P_{\text{ref(PV)}} - \frac{1}{m}\Delta\omega - D\frac{\mathrm{d}(\Delta\omega)}{\mathrm{d}t} \tag{7}$$

The active power droop coefficient m determines the sensitivity of the power reference to frequency deviations. The solution of the swing equation logic within this block yields the final active power reference, $P_{ref(PV)}$, which dynamically modulates the VSI's active power injection. where, J = 0.1028 pu (virtual inertia), $D = 0.02056Pu$ and $m = 0.0001$ (Yan et al., 2019, Alipoor et al., 2016)

b. Reactive Power Control (Q-V Droop):
This control block facilitates the VSI's participation in grid voltage regulation through a reactive power-voltage droop mechanism. The measured d-q components of the PCC voltage (V_{dgrid}, V_{qgrid}) are used to calculate the magnitude of the PCC voltage, V_{Pcc}. The voltage deviation from the nominal PCC voltage $V_{nominal(PCC)}$is then determined:

$$\Delta_V = V_{Pcc} - V_{nominal(PCC)} \tag{8}$$

$$Q_{ref(PV)} = Q_{Setpoint(PV)} - \frac{1}{n}\Delta V \quad (9)$$

where n is the reactive power droop coefficient (set to 0.0003) (Guerrero et al., 2010) and $Q_{Setpoint(PV)}$ is the reactive power setpoint at nominal voltage (typically 0 VAR). This calculation produces the reactive power reference, $Q_{ref(PV)}$, guiding the VSI's reactive power exchange.

iii. PWM Signal Generation Path

The active $(P_{ref(PV)})$ and reactive $(Q_{ref(PV)})$ power references generated by the outer loops are translated into precise switching commands for the VSI through a cascaded control structure, culminating in PWM signal generation.

a. Current Reference Generation:

The power references $(P_{ref(PV)}, Q_{ref(PV)})$ are converted into direct-axis (I_{dref}) and quadrature-axis (I_{qref}) current references using the measured grid voltage components (V_{dgrid}, V_{qgrid}) via standard power-voltage-current relationships (Chen and Chen, 2010).

b. Inner Current Control:

Fast and accurate tracking of the d-q current references is achieved using Proportional-Resonant (PR) controllers. Mathematically, Transfer Function,

$$G_{PR}(s) = K_p + \frac{K_{is}}{s^2 + w^2} \quad (10)$$

where, K_p = 1.2,K_i = 1000,w_o = 2 π x50 rad/s, Separate PR controllers are implemented for each axis. The d-axis controller processes the error,

$$I_{d(error)} = I_{d(ref)} - I_{d(meas)} \quad (11)$$

while the q-axis controller processes as[25],

$$I_{q(error)} = I_{q(ref)} - I_{q(meas)} \quad (12)$$

c. Decoupling and Feedforward:

The raw voltage commands from the PR controllers $(v_{dcommand(raw)}, v_{qcommand(raw)})$ are augmented with decoupling terms (to mitigate cross-coupling effects between the d and q axes,typically involving terms like $\omega_{grid(meas)} * L_f * I_{otheraxis}$ and potentially grid voltage feedforward terms (V_{dgrid}, V_{qgrid}). This yields the final d-q voltage commands $(V_{dcommand(final)}, V_{qcommand(final)})$, enhancing dynamic performance (Shao et al., 2023).

d. Inverse Park Transformation:

The final d-q voltage commands are transformed back into the three-phase stationary reference frame using the grid angle θ_{grid} (from the PLL). This Inverse Park Transformation generates the three-phase sinusoidal voltage references $V_{abc(ref)}$ (Anderson and Fouad, 2008).

2.2.3 Voltage Source Inverter (VSI) and Filter

The VSI converts the DC power from the solar PV system to AC power synchronized with the MHP-driven grid. Pulse-width modulation (PWM) generates gate signals for IGBTs, while LC filters (L=1mH,C=350 μF) suppress harmonics. This component ensures the seamless integration of solar PV into the AC microgrid (Trzynadlowski, 1996, Kshatri et al., 2024). Mathematically, PWM Reference voltage,

$$V_{ref} = V_{amp} sin(\omega + \delta) \quad (13)$$

$$FilterDesign; f_{cutoff} = \frac{1}{2\pi\sqrt{LC}} \quad (14)$$

Here, the values of L and C in our filter are: $L = 10^{-3} H \& C = 350 * 10^{-6} F$

3. Methodology

The 33.4 kW solar PV and 60 kW MHP systems are simulated in MATLAB/Simulink, synchronous generators, voltage source inverters, and LC filters being used to simulate grid synchronization and dynamic load-sharing for two 20 kW active + 5 kVAR reactive loads. Pivotal parameters such as irradiance (800–1000 W/m^2), flow rate ($0.12\ m^3/s$), and gross head (50 m) are selected to represent real conditions. The solution relies on transient response analysis, voltage/frequency deviation constraints ($< 5\%$ and $< 2\%$, respectively), and the assurance of uninterrupted power supply, adhering to grid stability standards through rigorous simulation of load switching and environmental variations.

3.1. Block Diagram

Figure 2 presents the complete architecture of the simulated Micro-Hydropower (MHP) - Photovoltaic (PV) hybrid AC microgrid, integrating both the power stage configuration and the detailed Voltage Source Inverter (VSI) control logic. The diagram illustrates the $60kW$ MHP system, comprising a synchronous machine managed by its governor and excitation controls, and the $33.4kW$ PV system, which includes the PV array, MPPT controller, boost converter, DC link, VSI, and LC filter. Both generation systems interface with the Point of Common Coupling (PCC) via respective line impedances, supplying power to both a fixed Load 1 and a switchable Load

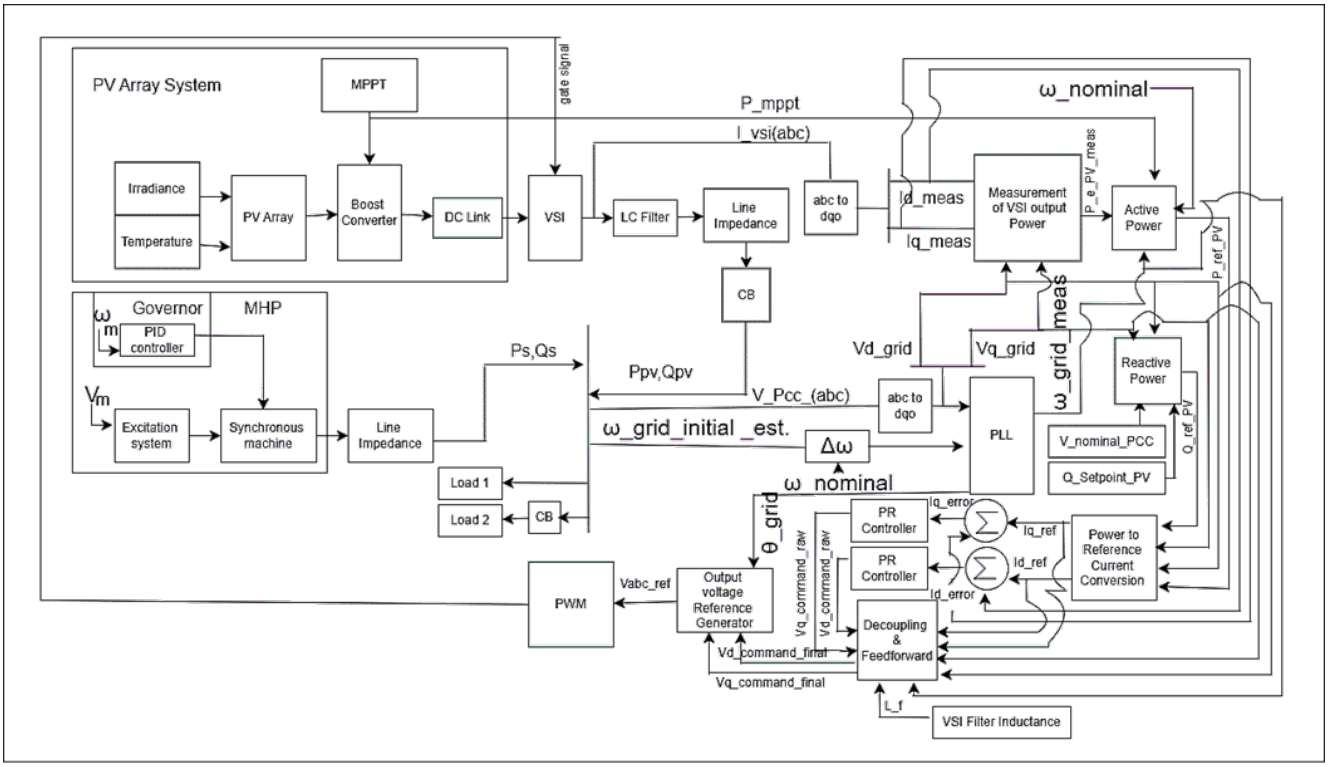

Figure 2. Overall System Design

2. A significant portion of the diagram details the VSI control system. Key components depicted include the Phase-Locked Loop (PLL) for grid synchronization deriving frequency ($\omega_{grid(meas)}$) and angle ($\theta grid$) from the PCC voltage ($VPcc(abc)$), coordinate transformations (abc to $dq0$), active power control (incorporating swing equation/P-f droop logic using $\omega_{grid(meas)}$andP_{mppt}), reactive power control (implementing Q-V droop based on VPcc magnitude), conversion to d-q current references, Proportional-Resonant (PR) based inner current control loops with decoupling, and the final Inverse Park Transformation generating the $V_{abc(ref)}$ signals for the PWM modulator. This comprehensive representation provides a clear visual map of the system components, their interconnections, and the sophisticated control strategy evaluated in this research.

3.2. Simulation Setup

3.2.1 Simulation of PV Model

A $33.4kW$ PV array is based on the electrical specifications and configuration (17 series modules/string, 9 parallel strings) . The model accounts for varying operational inputs of solar irradiance and temperature. Maximum power extraction is achieved using a Perturb and Observe (P&O) MPPT algorithm as shown in Figure 1, which controls the duty cycle of the DC-DC boost converter that

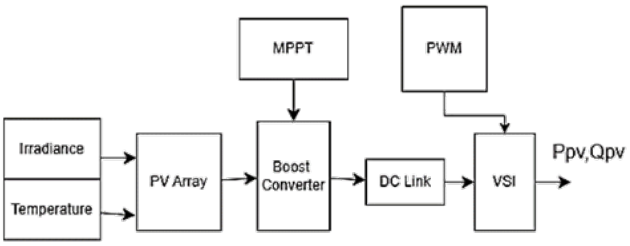

Figure 3. Block diagram of PV system

connects the array to the DC link. A DC link capacitor ($5000\mu F$) provides energy buffering and maintains the DC bus voltage (nominal $400V$). A three-phase Voltage Source Inverter (VSI) performs the DC/AC conversion. Crucially, the VSI model implements the detailed multi-loop control strategy described in Section II.B.2 and visually represented in Figure 2. This includes the PLL for synchronization, the swing equation-based droop for active power/frequency control, the Q-V droop for reactive power/voltage control, PR-based inner current controllers, and the PWM reference generation stages. An LC filter ($L = 1mH, C = 350\mu F$), is included at the VSI output to attenuate switching harmonics. The $33.4kW$ photovoltaic (PV) array is modeled based on a configuration of 9 parallel strings, each string comprising 17 series-connected modules. Each individual module consists of 60 cells and is characterized

by a maximum power output of 218.871 W under Standard Test Conditions (STC). The key electrical parameters per module in STC include an open-circuit voltage (V_{oc}) of $36.6V$, a short-circuit current (I_{sc}) of 7.97 A, a voltage at the maximum power point (V_{mp}) of 29.3 V, and a current at the maximum power point (I_{mp}) of 7.47 A. The temperature coefficient of (V_{oc}) is -0.36101 %/°C. For the single-diode model representation, the light-generated current (I_L) is 7.5592 A, the diode saturation current (I_D) is $2.9767 * 10^{-10}$ A, the diode ideality factor is 0.9893, and the shunt resistance (R_{sh}) is 316.6981 ohms.

3.2.2 Simulation of Micro-Hydropower Model

The MHP unit is modeled using a standard synchronous machine block representing the 60 kW generator. The 60 kW Micro-Hydropower (MHP) unit is modeled using a synchronous machine with a nominal power rating of 60000 VA and a nominal line-to-line voltage of 400V at 50 Hz. Its per-unit reactances are specified as: $X_d = 2.24$, $X'_d = 0.17$, $X''_d = 0.12$, $X_q = 1.02$, and$X''_q = 0.13$, with d-axis and q-axis transient characteristics based on short-circuit conditions. The machine time constants are $T'_d = 0.028s, T''_d = 0.007s, and T''_q = 0.007s$, and the stator resistance (Rs) is $0.037875pu$. Mechanical parameters include an inertia coefficient (H) of 0.1028 pu (s), a friction factor (F) of $0.02056pu, and 2 pole pairs$. Speed and frequency regulation for this MHP unit is provided by its governor, which employs a Proportional-Integral-Derivative (PID) controller. This PID controller is implemented in a parallel, discrete-time form using the compensator formula,

$$P + I.T_s \frac{1}{z-1} + D \frac{N}{1 + N.T_s \frac{1}{z-1}} \tag{15}$$

where T_s is the sample time of the inherited system. The specific gains for the governor PID are: Proportional (P) = 33.4604, Integral (I) = 7978.960, and Derivative (D) = -0.009983, with a derivative filter coefficient (N) of 585.340. The PID-based excitation system parameters are detailed in Sec. II.A

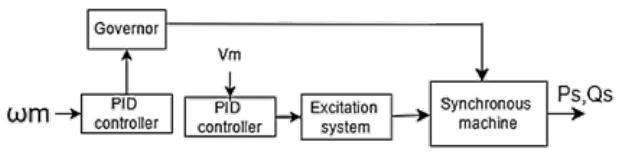

Figure 4. Block diagram of MHP system

3.2.3 System Loads

Two lumped loads, each rated at 20 kW active power and 5 kVAR reactive power, are connected to the PCC. Load 1 is constantly connected, while Load 2 is switched on at $t = 2\,seconds$ via a circuit breaker (CB) to simulate a load step event. The simulation begins with the MHP unit supplying Load 1 in steady state. At t= 0.6 s, the PV system is connected to the PCC and commences power injection, operating coordinately with the MHP based on the implemented control strategy. At $t = 2.0s$, $Load\,2$ is connected to the PCC, representing a 100% increase in the initial load demand, to evaluate the system's transient response and stability under disturbance.

4. Results and Discussion

The performance of the proposed power sharing control strategy for the MHP-PV hybrid AC microgrid was evaluated through simulations in MATLAB/Simulink. The simulation scenario initiates with the MHP system supplying a $20kW$ active and $5kVAR$ reactive load. At $t = 0.6$ seconds, the PV system is integrated to share this load. Subsequently, at $t = 2.0$ seconds, an additional identical load (20kW active, 5kVAR reactive) is connected to the PCC to assess the system's dynamic response to a significant load increase. The following subsections discuss the observed voltage regulation, current sharing, frequency stability, and active/reactive power distribution.

4.1. Voltage Regulation

The nominal three-phase AC voltage of the microgrid is $400V(line - to - line)$, corresponding to approximately 325V peak per phase or 230V RMS per phase. Figure 5 illustrates the terminal voltage waveforms for both the PV and MHP systems, demonstrating synchronized operation at this nominal level. Figure 6 further confirms the phase synchronization between the sources. Initially $(t < 0.6s)$, the MHP system maintains the voltage while supplying the $20kW/5kVAR$ load. Upon PV integration at $t = 0.6s$, and more significantly during the connection of the second load at $t = 2.0s$, transient voltage deviations occur. The most notable voltage dip was observed at $t = 2.0s$ when the additional load was introduced, with the phase voltage momentarily dropping to approximately 309V peak. The maximum voltage deviation (ΔV) was calculated as:

$$\Delta V = V_{max} - V_{min} V_{max} * 100\% = \frac{325 - 309}{325} * 100\% = 4.9\% \tag{16}$$

4.2. Current Waveforms

Figure 8 depicts the RMS currents supplied by the MHP and PV units. Initially $(t < 0.6s)$, the MHP exclusively

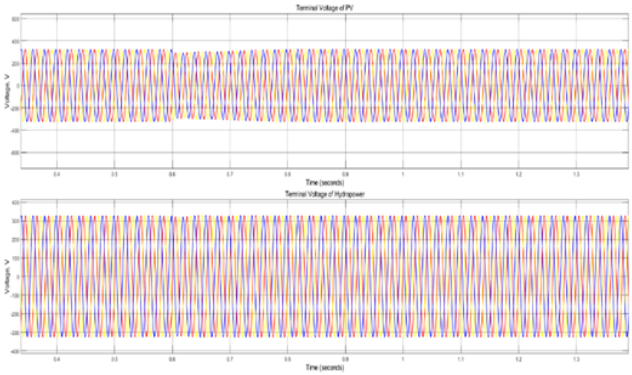

Figure 5. Terminal Voltage of PV and MHP

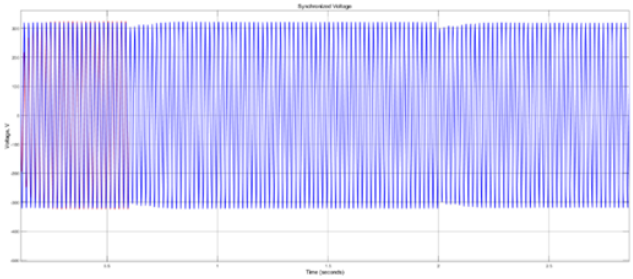

Figure 6. Synchronized Voltage

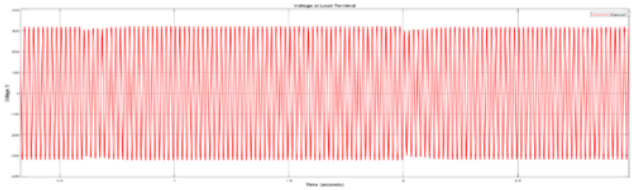

Figure 7. Voltage Supply to the Load

supplies the 20 $kW/5$ $kVAR$ load, drawing approximately. Upon PV integration at $t = 0.6s$, the PV system begins to contribute current, and the MHP's current contribution reduces as load sharing commences. After the addition of the second $20kW/5kVAR$ load at t $= 2.0s$, the total load current, shown in Figure 9, increases significantly. Under this full load condition $(40kW/10kVAR)$, the MHP supplies approximately 17A RMS, while the PV system supplies approximately $46ARMS$, demonstrating effective current sharing proportional to their power contributions and control settings.

4.3. Frequency Deviation

The nominal system frequency is $50Hz$. Figure 10 presents the microgrid frequency throughout the simulation. Initially, with the MHP supplying the first load, the frequency is maintained at $50Hz$. When the PV system integrates at $t = 0.6s$ and begins active power injection, a transient frequency increase to approximately 50.5 Hz is observed, after which the frequency rapidly settles back

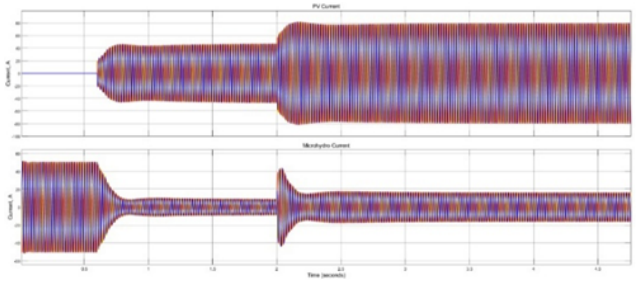

Figure 8. Current Supplied by PV and MHP

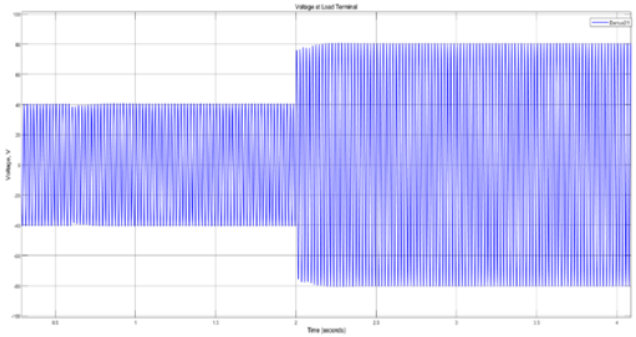

Figure 9. Current Supplied to Load

to 50 Hz. Upon the connection of the additional $20kW$ load at $t = 2.0s$, the frequency experiences a nadir of approximately $49.7Hz$ before recovering to the nominal $50Hz$ .The So, the deviation in the frequency obtained is:

$$\Delta f = f_{nom} - f_{min} * f_{nom} * 100\% = \frac{50 - 49.7}{50} * 100\% = 0.6\% \tag{17}$$

$$\Delta f = f_{nom} - f_{max} * f_{nom} * 100\% = \frac{[|50 - 50.5|]}{50} * 100\% = 1\% \tag{18}$$

These deviations are well within the typical acceptable operational limit $(e.g., \pm 2.5\%)$. Robust frequency regulation and rapid stabilization are achieved through the coordinated action of the MHP's governor and the P-f droop control (with virtual inertia from the swing equation) implemented in the VSI of the PV system.

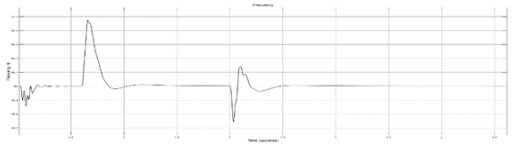

Figure 10. Synchronized Frequency

4.4. Active Power

Figure 11 details the active power contributions of the MHP and PV systems. For the first $0.6seconds$, the MHP

supplies approximately 24.1 kW to meet the 20 kW load demand and cover system losses. After PV integration at$t = 0.6s$, power sharing is evident: the PV system contributes approximately $22.3kW$, while the MHP reduces its output to approximately 3.4 kW, jointly supplying the $20kW$load plus losses. When the additional 20 kW load is connected at $t = 2.0s$ (total load demand $40kW$), the PV system increases its output to approximately 38.5 kW (approaching its available capacity under the simulated irradiance), and the MHP contributes approximately $5.2kW$. The combined generation of approximately $43.7kW$ effectively meets the 40 kW load demand and associated system losses, demonstrating the intended power sharing based on the droop settings and PV availability.

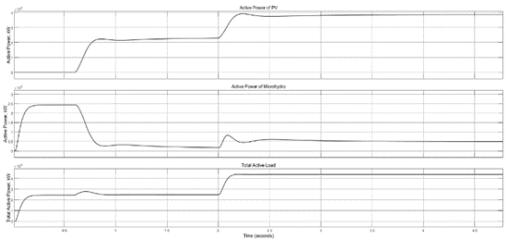

Figure 11. Active Power by PV and MHP

4.5. Reactive Power

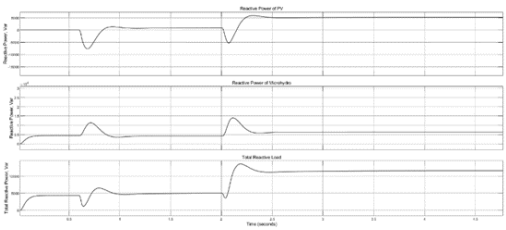

Figure 12. Reactive Power

The reactive power sharing dynamics are illustrated in Figure 12. Initially ($t < 0.6s$), with only the MHP active, it supplies approximately 4.3 kVAR to meet the $5kVAR$ load demand and system requirements. Upon PV integration at $t = 0.6s$, a transient behavior is observed where the PV system initially consumes approximately 7.5 kVAR for a very brief period, during which the MHP transiently increases its reactive power output to around $11kVAR$. Subsequently, the PV system begins to supply reactive power. Between $t = 0.6s$ and $t = 2.0s$, the PV contributes approximately 1.0 kVAR, and the MHP supplies approximately $3.5kVAR$, collectively meeting the $5kVAR$load. After the additional $5kVAR$ reactive load is introduced at $t = 2.0s$ (total reactive load demand $approx.10kVAR$), the PV system supplies approximately $5.7kVAR$, and the MHP supplies approximately $6.2kVAR$. The total reactive power supplied (approximately $11.9kVAR$) meets the 10 kVAR load demand and compensates for system reactive losses, indicating effective reactive power sharing governed by the Q-V droop characteristics of both the MHP's excitation system and the PV's VSI.

5. Conclusion

This research successfully developed and validated a robust power sharing control strategy for an islanded AC microgrid integrating a 60 kW micro-hydropower (MHP) unit with a 33.4 kW solar photovoltaic (PV) system, addressing the energy needs of remote regions such as those in Nepal. The implemented control architecture featured a swing equation-based droop controller for the PV system's Voltage Source Inverter (VSI) to provide virtual inertia and facilitate autonomous active power sharing, complemented by Q-V droop for reactive power management and Proportional-Resonant (PR) controllers for precise inner current loop regulation. Comprehensive MATLAB/Simulink simulations demonstrated the system's efficacy under dynamic conditions, including PV integration and significant step load changes (20kW active, 5kVAR reactive power). The hybrid system consistently maintained frequency within ±1% of 50 Hz and PCC voltage within ± 4.9% of nominal, while achieving effective and proportional active and reactive power distribution between the MHP and PV sources according to their designed droop characteristics and PV availability. This study thus contributes a validated control approach and a practical modeling reference, advancing the development of reliable, sustainable decentralized energy systems for remote electrification.

References

Abu-Sharkh, S., Arnold, R., Kohler, J., Li, R., Markvart, T., Ross, J., Steemers, K., Wilson, P., & Yao, R. (2006). Can microgrids make a major contribution to uk energy supply? *Renewable and Sustainable Energy Reviews*, *10*(2), 78–127.

Acakpovi, A., Hagan, E. B., & Fifatin, F. X. (2014). Review of hydropower plant models. *International Journal of Computer Applications*, *108*(18).

Ali, Z., Christofides, N., Hadjidemetriou, L., Kyriakides, E., Yang, Y., & Blaabjerg, F. (2018). Three-phase phase-locked loop synchronization algorithms for grid-connected renewable energy systems: A review. *Renewable and Sustainable Energy Reviews*, *90*, 434–452.

Alipoor, J., Miura, Y., & Ise, T. (2016). Stability assessment and optimization methods for microgrid with multiple vsg units. *IEEE Transactions on Smart Grid*, *9*(2), 1462–1471.

Alramlawi, M., Gabash, A., Mohagheghi, E., & Li, P. (2018). Optimal operation of hybrid pv-battery system considering grid scheduled blackouts and battery lifetime. *Solar Energy*, *161*, 125–137.

Amrollahi, M. H., & Bathaee, S. M. T. (2017). Techno-economic optimization of hybrid photovoltaic/wind generation together with energy storage system in a stand-alone micro-grid subjected to demand response. *Applied energy*, *202*, 66–77.

Anderson, P. M., & Fouad, A. A. (2008). *Power system control and stability*. John Wiley & Sons.

Ayasun, S., Eminoğlu, U., & Sönmez, Ş. (2014). Computation of stability delay margin of time-delayed generator excitation control system with a stabilizing transformer. *Mathematical problems in Engineering*, *2014*(1), 392535.

Ayres, D., & Zamora, L. (2024). Renewable power generation costs in 2023. *IRENA: Masdar City, United Arab Emirates*, 211.

Badal, F. R., Das, P., Sarker, S. K., & Das, S. K. (2019). A survey on control issues in renewable energy integration and microgrid. *Protection and Control of Modern Power Systems*, *4*(1), 1–27.

Baral, M., & Pun, P. B. (2022). Power sharing among parallel connected photovoltaic inverters with droop control in microgrid.

Bhattarai, U., Maraseni, T., Devkota, L. P., & Apan, A. (2024). Evaluating four decades of energy policy evolution for sustainable development of a south asian country—nepal: A comprehensive review. *Sustainable Development*, *32*(6), 6703–6731.

Chauhan, R. G., Rajput, S. K., & Singh, H. (2022). Additional power conservation in 200w power plant with the application of high thermal profiled cooling liquid & improved deep learning based maximum power point tracking algorithm. *Advances in Energy Research*, *8*(3), 185–202.

Chen, K.-L., & Chen, N. (2010). A new method for power current measurement using a coreless hall effect current transformer. *IEEE Transactions on Instrumentation and Measurement*, *60*(1), 158–169.

Erickson, R. W., & Maksimovic, D. (2007). *Fundamentals of power electronics*. Springer Science & Business Media.

Fachini, F., Bogodorova, T., Vanfretti, L., & Boersma, S. (2024). A microgrid control scheme for islanded operation and re-synchronization utilizing model predictive control. *Sustainable Energy, Grids and Networks*, *39*, 101464.

Gieras, J. F. (2016). *Electrical machines: Fundamentals of electromechanical energy conversion* (1st). CRC Press. https://doi.org/10.1201/9781315371429

Guerrero, J. M., Vasquez, J. C., Matas, J., De Vicuña, L. G., & Castilla, M. (2010). Hierarchical control of droop-controlled ac and dc microgrids—a general approach toward standardization. *IEEE Transactions on industrial electronics*, *58*(1), 158–172.

Khazali, A., Rezaei, N., Saboori, H., & Guerrero, J. M. (2022). Using pv systems and parking lots to provide virtual inertia and frequency regulation provision in low inertia grids. *Electric Power Systems Research*, *207*, 107859.

Kshatri, A., Dhami, S., & Bhatta, A. (2024). Power quality enhancement strategy in grid connected dual voltage source inverters supplying various loads. *OODBODHAN*, *7*, 23–30.

Martínez-Velasco, J. A. (Ed.). (2010). *Power system transients: Parameter determination* (1st) [MATLAB® is a trademark of The MathWorks, Inc.]. CRC Press. https://doi.org/10.1201/9781420065305

Neupane, D., & Gurung, S. (2022). Power management in solar pv-microhydro hybrid system using power angle control strategy with syncronverter.

Saranya, S., Sathyamoorthi, S., & Gandhiraj, R. (2015). A fuzzy logic based energy management system for a microgrid. *ARPN Journal of Engineering and Applied Sciences*, *10*(6), 2663–2669.

Shao, B., Xiao, Q., Xiong, L., Wang, L., Yang, Y., Chen, Z., Blaabjerg, F., & Guerrero, J. M. (2023). Power coupling analysis and improved decoupling control for the vsc connected to a weak ac grid. *International Journal of Electrical Power & Energy Systems*, *145*, 108645.

Trzynadlowski, A. M. (1996). An overview of modern pwm techniques for three-phase, voltage-controlled, voltage-source inverters. *Proceedings of IEEE International Symposium on Industrial Electronics*, *1*, 25–39.

Usman, A. A., & Abdulkadir, R. A. (2015). Modelling and simulation of micro hydro power plant using matlab simulink. *International journal of advanced technology in Engineering and Sciences*, *3*, 260–272.

Yan, X., Mohamed, S. Y., Li, D., & Gadalla, A. S. (2019). Parallel operation of virtual synchronous generators and synchronous generators in a microgrid. *The Journal of Engineering*, *2019*(16), 2635–2642.

Published by JScE as Proceedings of 4th International Conference on Role of Energy on Sustainable Social Development (RESSD-2025), 29-30 May, 2025, Kathmandu, Nepal

This page is intentionally left blank.